International Journal of Microwave and Wireless Technologies, 2014, 6(6), 645–651.
doi:10.1017/S1759078714000269

RESEARCH PAPER

Comparative analysis of radial and axial power output in relativistic magnetron and effect of dielectric side-walls introduced in the resonator on dominant operating mode

AYUSH SAXENA[1], RAJU BARAKADE[1], NAVDEEP M. SINGH[1] AND ANKUR PATEL[2]

A comparative analysis of radiated power in relativistic magnetron is done using particle-in-cell simulations performed on Magic3d code developed by ATK Mission Systems. The Resonator with dielectric side-walls (DSW) is compared with no-side wall (NSW) configuration having same input parameters and resonator dimensions. Observations and comments have been made on the output power, obtained both axially and radially, taking into consideration π as well as 2π modes of operation for both configurations. The DSW assist in π-mode operation at 3.3 GHz and delivers radial peak power output of ~2.5 GW, which is more than ~1.5 GW, the radial peak power for the NSW case. The NSW case operates in dominant 2π mode (radially) at 5.68 GHz with axial power radiated at dominant π-mode frequency. The electron kinetic energies and their distribution in the cavity are discussed together with the dynamic behavior of particles, which result in spokes formation.

Keywords: Modeling, Simulation and characterizations of devices and circuits, Antennas and propagation for wireless systems

Received 3 October 2013; Revised 2 February 2014; first published online 11 March 2014

I. INTRODUCTION

A relativistic magnetron is an important high-power microwave energy source. It can operate on a single-shot high-voltage (HV) pulse of nanoseconds duration, as well as, on multiple, short-duration HV pulses and produces output power in the order of hundreds of megawatts to several gigawatts [1, 2]. The magnetron under consideration is the MIT A6 vane-type, although with modified cavity parameters. Improvements in the power efficiency is reported in [3, 4], using the method of axial power extraction with π as dominant mode of operation. Most often, only the π-mode frequency lies in the S-band (2–4 GHz) as the 2π-mode frequency is nearly twice that of the π mode, hence, for S-band operation it is desirable for magnetron to operate in the π mode. The A6 magnetron operation having resonator vanes partially loaded with low-loss dielectric material has been reported in [5, 6], operating in 2π mode with high radial output power and low start up time in comparison to the unfilled side resonators. The motivation of this paper is to study the design aspects of a relativistic magnetron and comment on the radiated output power both in the axial and radial directions.

A modified configuration of relativistic magnetron with axial power output or diffraction output has been proposed in [7] and three-dimensional particle-in-cell simulations using simulation-code MAGIC were carried out to demonstrate the effectiveness of the modified configuration. Power in relativistic magnetrons is extracted radially through single or multiple iris of different width. In [8], it has been shown that in general output power and efficiency increase approximately linearly with increasing iris width until the total Q becomes too low. Beyond this point, mode competition or switching occurs and efficiency decreases.

II. THEORETICAL BACKGROUND

The schematic of a typical A6 magnetron is shown in Fig. 1. The anode consists of vanes and slots and forms the slow-wave structure (SWS), which makes the RF wave inside to resonate and grow [9]. The SWS is different from a fast-wave structure (FWS), as a FWS has phase velocity greater than the speed of light. The fundamental mode frequency is determined by the capacitive and inductive values of the SWS. For a six vane magnetron ($N = 6$) there exist six operating modes ($n = 1, 2, \ldots, 6$), with $N/2$ being the π mode and $n = 6$, the 2π mode.

[1]Electrical Engineering Department, Veermata Jijabai Technological Institute, H.R. Mahajani Marg, Matunga, Mumbai, India. Phone: +91 9773728838
[2]Pulsed Power Division, Bhabha Atomic Research Centre, Mumbai, India
Corresponding author:
A. Saxena
Email: ayushsaxena3108@gmail.com

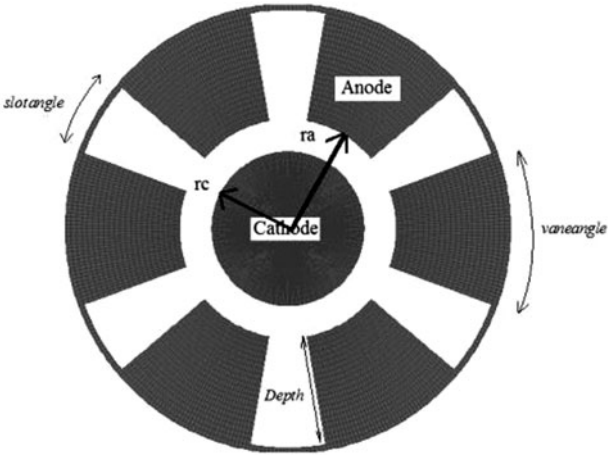

Fig. 1. Basic schematic of the A6 magnetron resonator.

In [10], theoretical formula for π-mode frequency based on equivalent circuit method has been derived as a function of structure dimensions. Also, in [1] equivalence of admittance of the resonator vanes and anode–cathode (AK) cylindrical gap region is used to obtain resonant frequency for various modes of magnetron operation. The fundamental modes are considered to be the π and 2π as all other modes are degenerate modes [2].

For a given voltage, the applied magnetic field must be large enough to form the initial electron sheath (Brillouin layer) around the cathode without allowing breakdown of the AK gap. The Brillouin sheath originates from cathode and extends to some distance (hub) toward the anode. The RF fields in the SWS cause instabilities in the sheath by means of Reyleigh instabilities [10, 11]. The critical magnetic field to prevent breakdown of the AK gap is called the Hull field, given as [2],

$$B_{Hull} = \frac{mc}{ed}\sqrt{\gamma^2 - 1}, \tag{1}$$

where, m and e are the electron mass and charge, c is the velocity of light, V is the applied voltage, $d = (r_a^2 - r_c^2)/2r_a$ is the effective AK gap and $\gamma = 1 + eV/mc^2$. A formula for high-power magnetron efficiency with full-relativistic effects (changes in γ) is derived and discussed in [12].

The electric field (E_r) causes radial motion to the electrons in a straight line from cathode to anode, whereas, the magnetic field (B_z) causes azimuthal rotation. The effective velocity of electron (v_e) for resonance is given as,

$$v_{ph} = \frac{r_a\omega}{n} \approx v_e = \frac{E_r}{B_z}, \tag{2}$$

where, ω is the angular frequency, v_{ph} is the phase velocity of SWS and n is the mode number.

There should be a maximum threshold field B_z to allow resonance between moving electrons and the SWS. The relationship between the applied voltage and the magnetic field at such threshold is called the Bunemann–Hartree condition, given as,

$$B_z = \frac{nmc^2}{2\pi \times freq \times r_a ed}\left(\frac{eV}{mc^2} + 1 - \sqrt{1 - \left(\frac{2r_a\pi freq}{nc}\right)^2}\right), \tag{3}$$

The operating point for the device must lie between the Hull and Hartree curves for a particular mode. The input voltage and the preset magnetic field intensity, is obtained by the Hull and Bunemann–Hartree criteria (V–B_z plot) [2].

There is a significant influence of the structural aspect ratio, α in selecting the mode of operation. Generally accepted [13] criteria is that small α devices ($\alpha < 1$) tend to operate in single mode at π-mode frequency. The tendency to operate in multimode grows at higher α-values, and large-α devices can simultaneously support a number of different modes including π and 2π, etc. Also, to keep magnetic field values below certain threshold (0.6 Tesla in this paper), the AK gap needs to be increased from the MIT A6 values, if voltage of operation is to be kept at a certain constant value. The increase in AK gap also assists in the three-spoke formation (π mode).

III. SIMULATION AND RESULTS

The resonant structure of relativistic magnetron consists of six cavities with an azimuthal spacing of 60°. The radius of cathode (r_c) and radius of anode (r_a) are 1.2 and 2.0 cm, respectively. The AK gap is 0.8 cm, resonator vane depth is 2 cm and the length of the resonator in the z-direction is 7.2 cm. The cross-sectional schematic of the three-dimensional model of A6 relativistic magnetron is shown in Fig. 2.

The operating voltage is set to 400 kV and 0.58 T magnetic field strength is applied to the total simulation volume, which is in accordance with the operating region from the V–B_z curves for Hull and Bunemann–Hartree conditions for the π-mode operation. The radial power is observed at an open vane, whereas, a probe is used for axial extraction. Copper is used as material for cathode as well as anode. The dielectric side-wall (DSW) is of porcelain to withstand high electrical stresses.

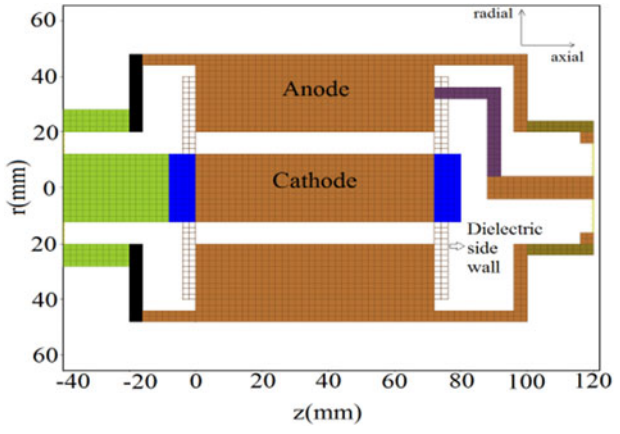

Fig. 2. Schematic representation of the relativistic magnetron with DSW (six vanes).

https://doi.org/10.1017/S1759078714000269 Published online by Cambridge University Press

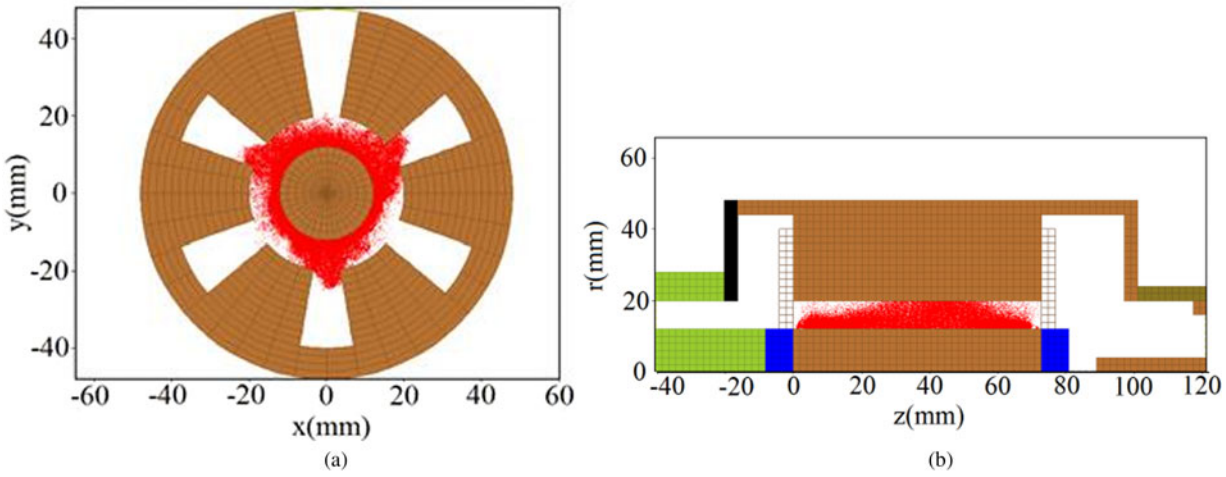

Fig. 3. (a) Particle phase space at 50 ns for DSW (r–phi plane). (b) Particle phase space at 50 ns for DSW (z–r plane).

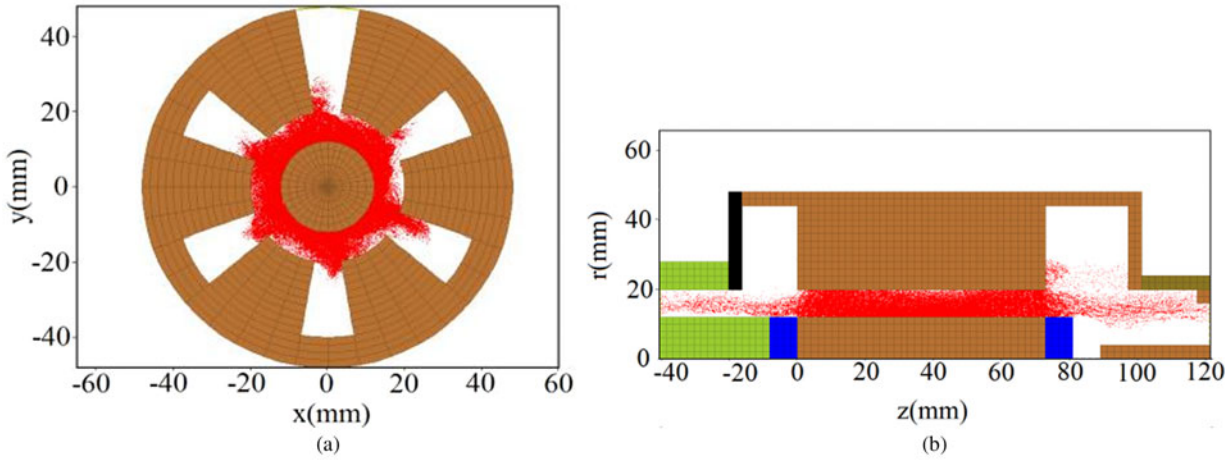

Fig. 4. (a) Particle phase space at 50 ns for NSW (r–phi plane). (b) Particle phase space at 50 ns for NSW (z–r plane).

The results are categorized into four sub-sections. Section A demonstrates the particle phase space and formation of modes (spokes) for both configurations, relativistic magnetron with DSW and no-side wall (NSW) cases. Section B compares the radial output powers and corresponding dominating frequencies. Time–frequency analysis has also been done to demonstrate the time of occurrence and sustained frequency components. Section C is similar to the second just that axial power outputs are analyzed. Section D deals with the particle characteristics including their distribution and energies at different modes of operation.

A) Particle phase space and mode formation

The phase space of particles inside the magnetron with DSW at 50 ns is shown in Figs 3(a) and 3(b). As discussed earlier, fixing the operating point (voltage and magnetic field values) from V–B_z curve for a certain mode or frequency is critical, as different modes operating at different frequencies might lie in the same operating region leading to mode-competition and reduced efficiencies. Figure 3 shows a dominant three-spoke formation, with no particles escaping out of the resonator in axial direction due to the introduction of DSW.

The phase velocity of the SWS is increased by the introduction of DSW and so is the resonant frequency for the dominant modes. The resonant frequencies for π and 2π modes are ~3.3 and 6.6 GHz, respectively. For the same operating point (400 kV, 0.58 Tesla), NSW case shows six-spokes forming inside the resonator at 50 ns (Figs 4(a) and 4(b)). Here, more electrons are escaping out in the axial direction. The resonant frequencies for π and 2π modes are ~2.84 and 5.68 GHz, respectively.

Although, the applied HV pulse is of 400 kV, the effective voltage observed at the source is 500 kV for DSW case and approximately 450 kV for NSW case. As a result, the electron velocity increases as per equation (2) so as to follow the increased RF phase velocity of the SWS. The fourier transform (FFTs) of the source voltages show that dominant frequency for the DSW case is the π-mode frequency of 3.3 GHz, whereas, for NSW case it is the 2π mode which is dominant with frequency 5.68 GHz.

B) Radial power output

The radial power has been calculated in a single vane through a 72 mm × 16.6 mm rectangular section. Although there is

https://doi.org/10.1017/S1759078714000269 Published online by Cambridge University Press

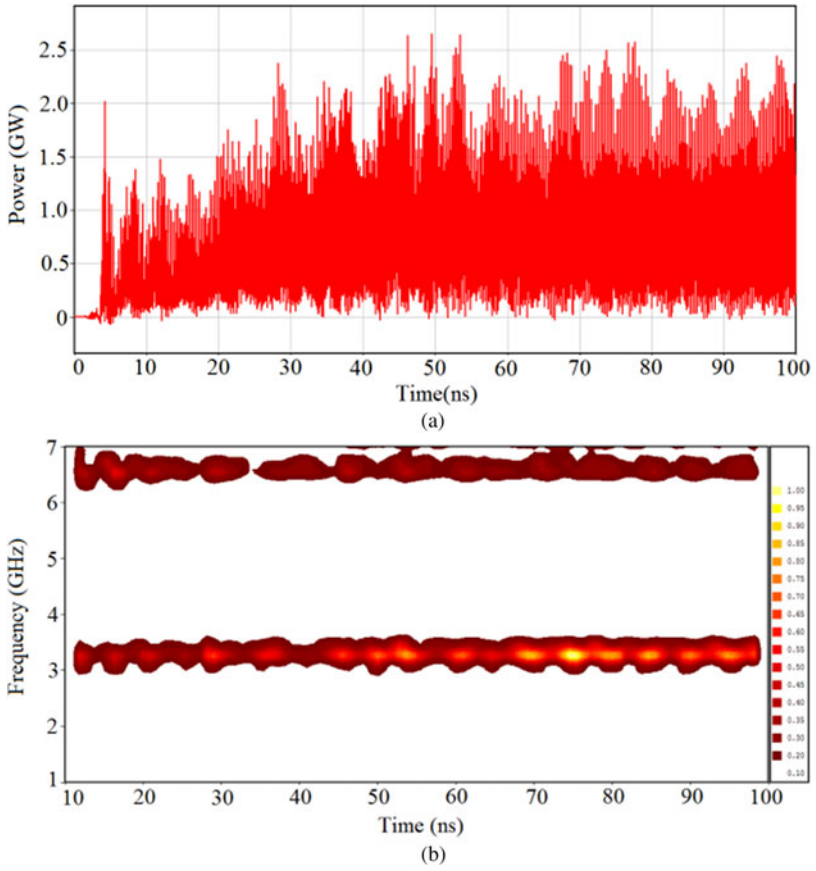

Fig. 5. (a) Radial power output (DSW). (b) Time–frequency relation showing dominant pi mode frequency 3.3 GHz (DSW).

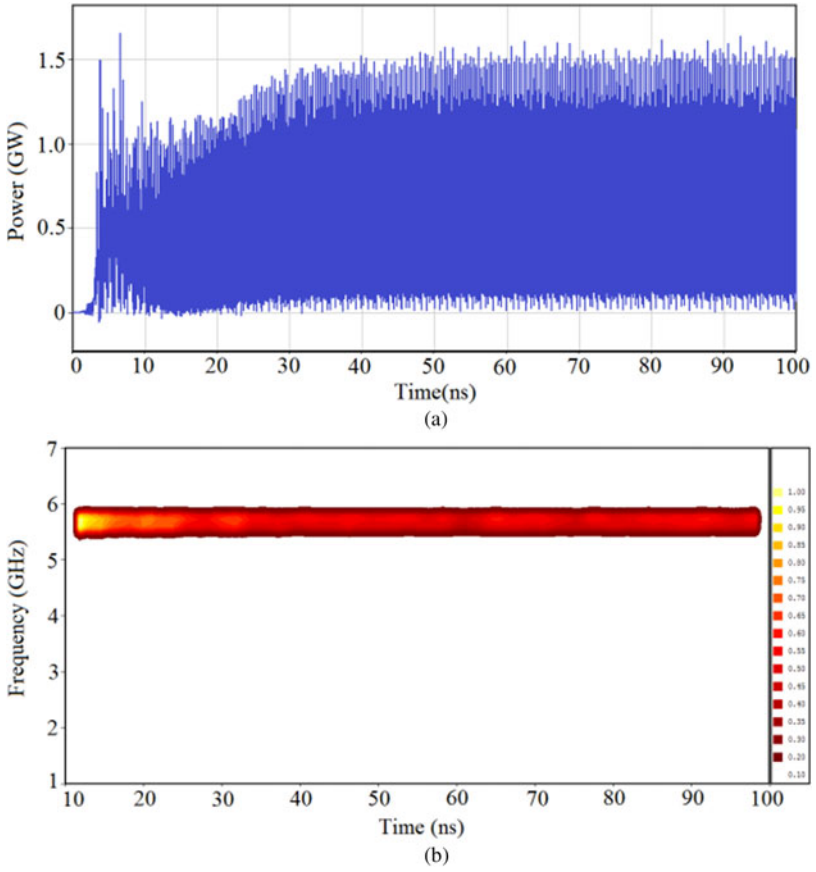

Fig. 6. (a) Radial power output (NSW). (b) Time–frequency relation showing dominant 2π mode frequency 5.68 GHz (NSW).

https://doi.org/10.1017/S1759078714000269 Published online by Cambridge University Press

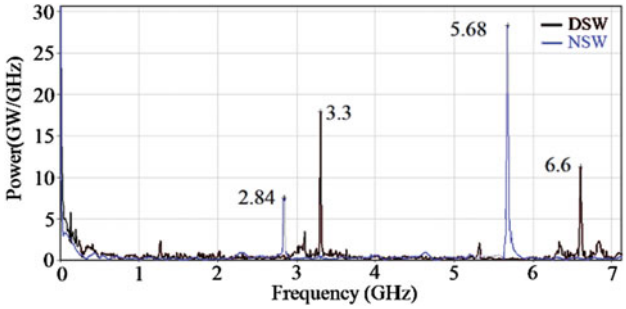

Fig. 7. FFT of the radial power output for DSW and NSW, showing comparison of dominant frequency components.

mode competition observed in DSW case, the dominant mode is the π mode with peak output power ~2.5 GW and average power around 900 MW (Fig. 5(a)) is observed which is greater than the NSW case operating at dominant 2π frequency with peak power ~1.5 GW and average power around 600 MW (Fig. 6(a)). Figure 5(b) shows the time–frequency plot for DSW case to analyze the frequency content of the radiated power in time. This can be compared with the time–frequency plot of radiated power for NSW case shown in Fig. 6(b).

The FFTs of the radial power for both the cases is compared in Fig. 7 and the dominant frequencies for DSW and NSW cases can be distinguished. There is a clear indication that the introduction of DSW tend to pull-back the operation mode from 2π to π resulting in more output power being observed at radial port. The time–frequency spectrogram (Fig. 5(b)) give further insight into the existing modes.

C) Axial power output

The average axial power from Fig. 8(a) (~20 MW) is nearly one-fifth of the NSW case (Fig. 9(a)). Although the dominant frequency is of 2π mode, various modes coexist (Fig. 8(b)) causing reduction in radiated power. An interesting observation is that the axial power for NSW case is at dominant π mode, which is in contradiction with the radial power radiated at dominant 2π mode and formation of six spokes (Fig. 9(b)).

One reason may be the inappropriate axial radiation cross-section area and the probe geometry. In spite of the contradiction, a major observation is that the radial power is generally more than the axially radiated power whether magnetron is operating in π or 2π mode or DSW are introduced or not. Although, the axial power for NSW case is radiated at dominant π mode, there co-exists the 2π mode as clear from Figs 9(b) and 9(c).

D) Electron motion

The average energy of the particles [14] within the volume is calculated by the relation,

$$Energy = \sum_i (\gamma_i - 1) \times mc^2 N_i / \sum_I N_i, \qquad (4)$$

which refers to statistical moments of sums and products of the particle's position and momentum variables in Cartesian coordinates. These statistical quantities are renormalized to the total number of physical particles. The average energy of all particles over the 100 ns simulation runtime lies between 100 and120 keV for both cases, with energy values being slightly higher for DSW case (~5 keV).

The comparison between the frequency of particles is shown in Fig. 10(a). Note the dominance of π-mode

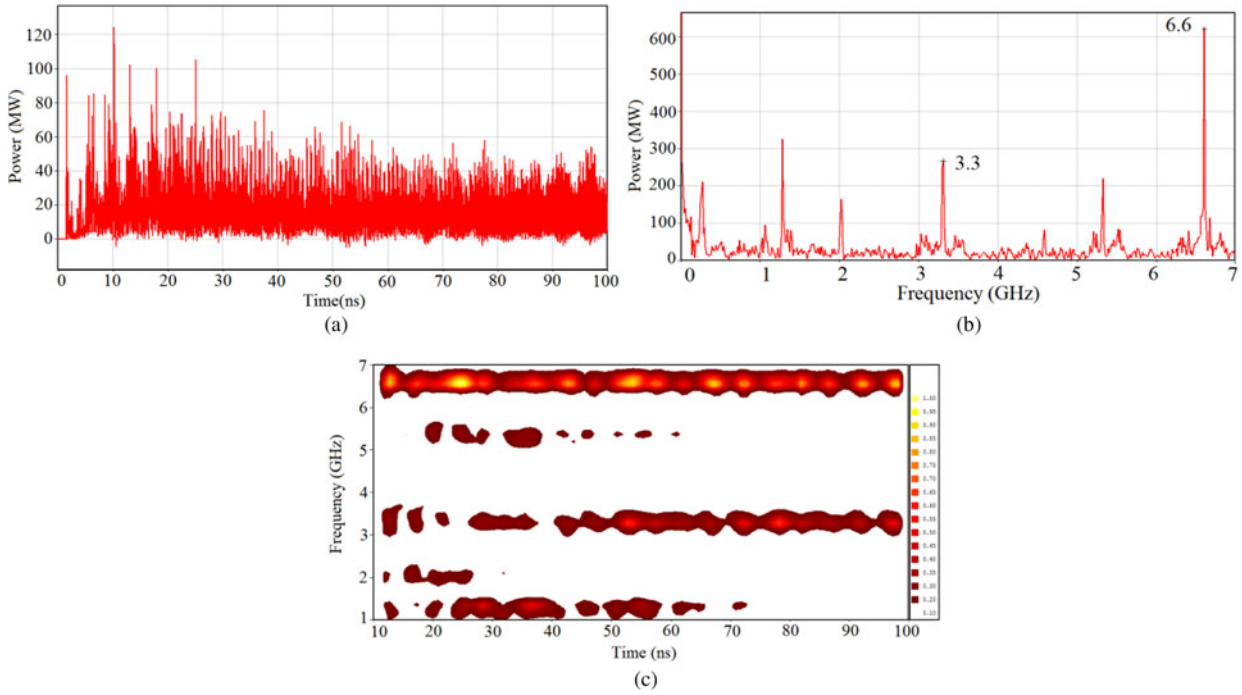

Fig. 8. (a) Axial power output (DSW). (b) FFT of axial power output (DSW). (c) Time–frequency relation of axial power output showing existence of various modes (DSW).

https://doi.org/10.1017/S1759078714000269 Published online by Cambridge University Press

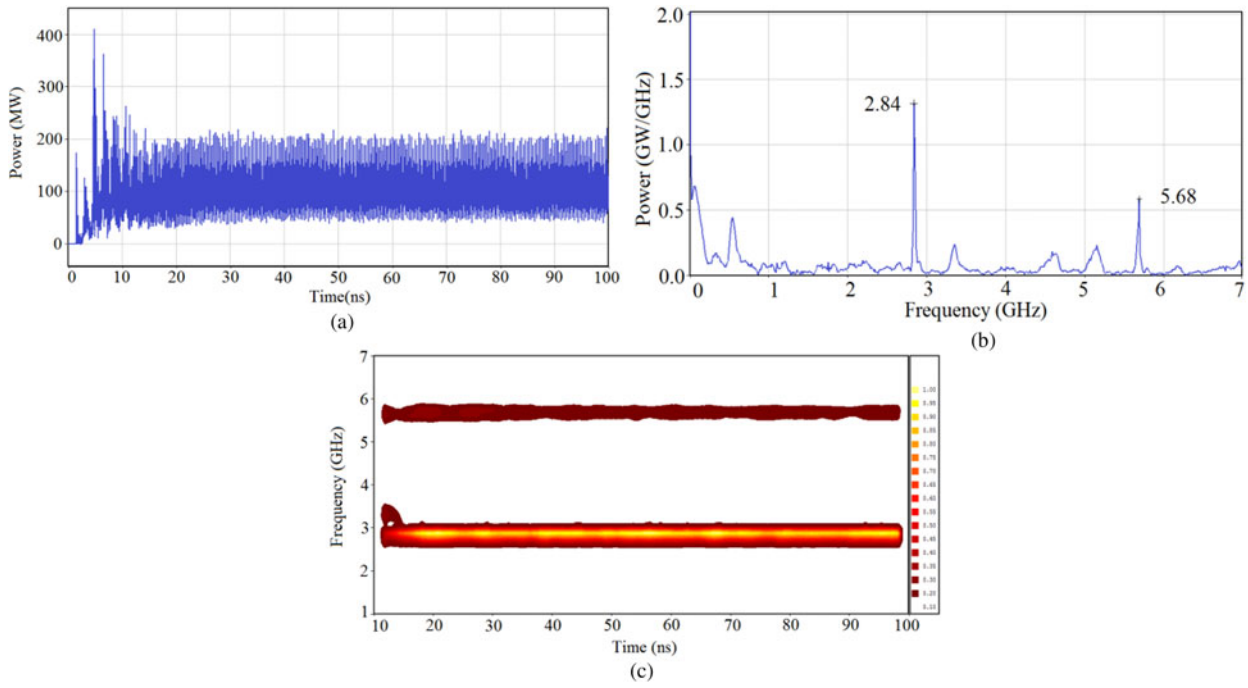

Fig. 9. (a) Axial power output (NSW). (b) FFT of axial power output (NSW). (c) Time–frequency relation of axial power output showing existence of π and 2π modes with dominant π-mode frequency 2.84 GHz (NSW).

frequency for the DSW case. The distribution of particles in the resonator for DSW case at 30 ns is shown in Fig. 10(b). The three peaks demonstrate the formation of three spokes.

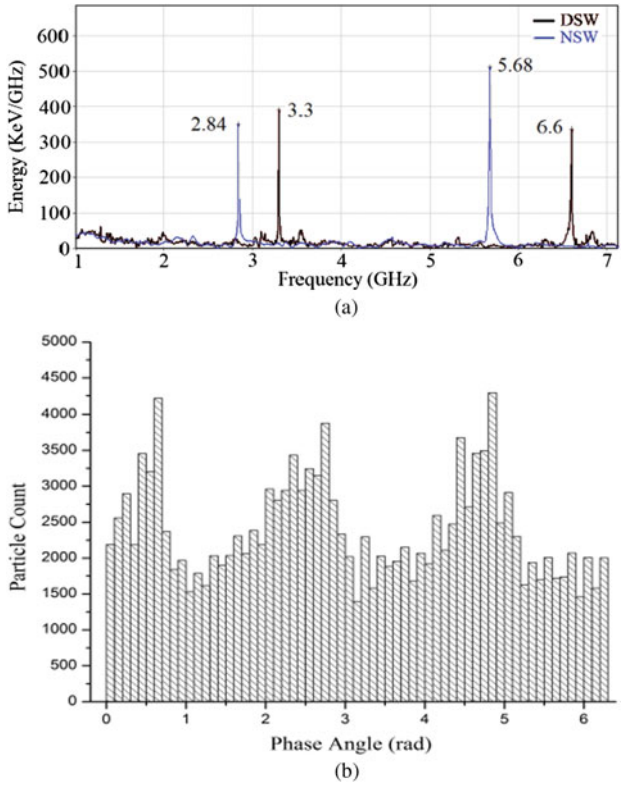

Fig. 10. (a) Comparison of FFT of the average energy of electrons for both cases. (b) Distribution of particles for DSW case at 30 ns.

IV. CONCLUSION

Introduction of DSW show improvement in π-mode operation and peak radial power output. The motivation is to remove the ambiguity in spoke formation and its connection with the peak powers obtained. Radial power extraction is supposed to give better power efficiency as compared to axial extraction, whatever be the mode of operation π or 2π. Study of the electron motion and patterns in their characteristics is the key to the operation of electron devices such as relativistic magnetron and computer-based simulations aid in getting that insight.

ACKNOWLEDGEMENTS

The authors would like to thank the team of Centre of Excellence, Complex and Nonlinear Dynamical Systems (COE-CNDS), VJTI, for their active support. Special mention for Dr. Amitava Roy for sharing his expert opinion on the subject.

REFERENCES

[1] Collins, G.B.: Microwave Magnetrons, McGraw-Hill Book Company, Inc., New York, 1948.

[2] Benford, J.; Swegle, J.; Schamiloglu, E.: High Power Microwaves, 2nd ed., Taylor & Francis, New York, London, 2007.

[3] Fuks, M.I.; Schamiloglu, E.: 70% efficient relativistic magnetron with axial extraction of radiation through a horn antenna. IEEE Trans. Plasma Sci., **38** (6) (2010), 1302–1312.

https://doi.org/10.1017/S1759078714000269 Published online by Cambridge University Press

[4] Li, W. et al.: Experimental demonstration of a compact high efficient relativistic magnetron with directly axial radiation. Phys. Plasmas, **19** (2012), 013105.

[5] Hashemi, S.H.A.: Dielectric cavity relativistic magnetron. Appl. Phys. Lett., **96** (8) (2010), 081503-1–081503-3.

[6] Maurya, S.; Singh, V.V.P.; Jain, P.K.: Study of output performance of partially dielectric loaded A6 relativistic magnetron, IEEE Trans. Plasma Sci. **40**(4) (2012), 1070–1074.

[7] Daimon, M.; Jiang, W.: Modified configuration of relativistic magnetron with diffraction output for efficiency improvement. Appl. Phys. Lett., **91** (2007), 191503; doi: 10.1063/1.2803757.

[8] Raymond, W.; Lemke, T.; Genoni, C.; Spencer, T.A.: Effects that limit efficiency in relativistic magnetrons. IEEE Trans. Plasma Sci. **28** (3) (2000).

[9] Kaup, D.J.: Theoretical modeling of an A6 relativistic magnetron. Phys. Plasmas, **11** (2004), 3151; doi: 10.1063/1.1710518.

[10] Fan, Y.-W.; Liu, J.; Zong, H.-H.; Shu, T.; Li, Z.-Q.: Theoretical investigation of the fundamental mode frequency of A6 magnetron. J. Appl. Phys., **105** (2009), 083310.

[11] Drazin, P.G.; Reid, W.H.: Hydrodynamic Stability, *Cambridge University Press*, New York, 1981, Chap. 4.

[12] Riyopoulos, S.: Efficiency reduction caused intense rf-induced E × B drift during relativistic magnetron operation. Phys. Plasmas, **6** (1999), 1344; doi: 10.1063/1.873714.

[13] Sayapin, A.; Shalapakovski, A.: Transient operation of the relativistic magnetron with radial output. J. Appl. Phys., **109** (2011), 063301.

[14] Ludeking, L.; Woods, A.; Cavey, L.: Magic User Manual 3.2, AlliantTechsystems, USA, 2011.

Ayush Saxena received a degree in Electrical Engineering from the U.P. Technical University, India, in 2007 and received his Master's degree in Control Systems from Mumbai University, in 2009. He is currently working as a Senior Research Fellow in VJTI, India. His research interest includes modeling of high-power microwave devices, partial discharges, plasma cavities, dynamical systems and control, and elements from particle physics.

Raju Barakade completed B.E. degree in electronics and Tele-communication from Shivaji University, Kolhapur, India, in 2008. He received the M.Tech. degree in Control Systems from VJTI, in 2013. His area of interest includes microwave engineering and antenna design.

Navdeep M. Singh received the M.Tech. degree in systems and control engineering from IIT, Bombay, in 1983. He received his Ph.D. degree in Electrical Engineering from IIT Bombay, in 1990. He is currently working as a Professor in Electrical Engineering Department, VJTI. He is also the coordinator of COE-CNDS, VJTI. His research interest includes the areas of nonlinear control system dynamics and design, robotics, topological, and geometrical aspects of linear time invariant systems.

Ankur Patel received his B.E. degree from Sardar Patel University, Mumbai, in Electronics and Communication. He received the M.Tech. degree from Homi Bhabha National Institute, India, in Engineering Physics (Accelerators), in 2009. He is currently working as a Scientific Officer on the Pulsed power systems, HPM diagnostics, Capacitor charging power supply, and HPM sources.

https://doi.org/10.1017/S1759078714000269 Published online by Cambridge University Press